Springer

Journal of
Mechanical
Science and
Technology

Journal of Mechanical Science and Technology 22 (2008) 338~349

www.springerlink.com/content/1738-494x

Performance analysis of air-cooled microchannel absorber in absorption-based miniature electronics cooling system

Yoon Jo Kim*, Yogendra K. Joshi and Andrei G. Fedorov

The George W. Woodruff School of Mechanical Engineering Georgia Institute of Technology Atlanta, GA 30332

(Manuscript Received April 16, 2007; Revised August 29, 2007; Accepted August 29, 2007)

Abstract

Theoretical analysis and simulation of performance of an air-cooled microchannel absorber is reported in this study. It is shown that the air-cooled microchannel absorber can be integrated into an absorption-based miniature electronics cooling system by which the chip junction temperature can be maintained near room temperature, while removing 100 W of heat load. Water/LiBr pair is used as the working fluid and refrigerant vapor is intended to counter-currently flow against aqueous LiBr solution flow. Parametric study is carried out to determine the effects of several operating parameters, including inlet temperature and mass flow rate of the coolant, and inlet temperature of LiBr solution. To facilitate the air-cooling of microchannel absorber, an offset-strip-fin array is adopted, by which enhanced air-side heat transfer coefficient and large heat transfer area are obtained. The performance of the air-cooled absorber is compared to liquid-cooled absorber.

Keywords: Absorber; Microchannel; Electronics cooling; Offset-strip-fin

1. Introduction

Recent advances in semiconductor technologies have been accompanied by a rapid increase in power density levels from high performance chips such as microprocessors. According to the International Technology Roadmap for Semiconductors (ITRS), by the year 2009 these chips are expected to dissipate power at an average flux of 64 W/cm^2, while keeping the maximum junction temperature of near 90^{o}C [1]. Conventional packaging solutions, which use convective air-cooling techniques, are facing difficulties in removing such large heat fluxes under the limited space allocated to thermal management. Further increase in cooling power will require insertion of a "negative" thermal resistance into the heat flow path, which can be achieved by the use of refrigeration [2]. Mongia et al. [2] developed a small scale vapor compression system for electronics cooling within a notebook computer that can remove 50 W of heat from the central processing unit (CPU) with a coefficient of performance (COP) of about 2.25 and the minimum junction-to-fluid thermal resistance of 0.25 K/W. Drost and Friedrich [3] developed a mesoscale water/LiBr absorption-based heat pump system for portable and distributed space conditioning applications with 350 W of cooling capacity.

One of the major advantages of an absorption-based heat pump system is the use of a 'chemical compressor' which consists of an absorber, a liquid pump, a solution heat exchanger and an expansion device. The condensation/absorption process in the absorber and vaporization/desorption process in the desorber make use of a liquid pump feasible to support pressure difference between condenser and evaporator. Although the presence of an absorber and a desorber increases the overall system volume, the displacement volume and power consumption for liquid compression are much smaller than those for

*Corresponding author. Tel.: +1 404 385 1880, Fax.: +1 404 894 8496
E-mail address: yoonjo.kim@me.gatech.edu
DOI 10.1007/s12206-007-1034-5

vapor compression, so that chemical compression is more favorable to miniaturization than mechanical vapor compression.

The absorber is widely acknowledged as the "bottleneck" which defines the viability of the entire absorption cycle [4] and also as the most critical component in absorption heat pump system in terms of cycle performance and system cost [5]. Significant efforts toward modeling the absorption process have been undertaken, as reviewed by Killion and Garimella [5]. The absorber analysis can be classified into two categories by working fluid pair: water/LiBr and ammonia/water. Since LiBr is essentially non-volatile, the water vapor is pure so that there is no resistance to mass transfer in the vapor phase during the absorption process. In contrast, due to the volatility of both components in an ammonia/water system, both ammonia and water may be present in the vapor phases and thus the potential for mass transfer resistance in the vapor phase exists [5]. Also, heat transfer and mass transfer coefficient correlations and/or heat-mass transfer analogy make one-dimensional simplified models feasible for exploring the absorption process with sufficient accuracy.

Patnaik et al. [6] developed a one-dimensional simplified model for water/LiBr steady vertical-film absorption that applies to both laminar and wavy-laminar film flow regimes. Meacham and Garimella [7] also presented experimentally validated a one-dimensional predictive model for ammonia/water absorption process in a novel microchannel absorber for residential and light commercial applications. A compact heat exchanger, which allows mini- or microchannel flow path, mostly provides high area density (generally higher than 700 m^2/m^3) as well as high heat transfer coefficients [8]. Kang et al. [8] compared the performance of falling film and bubble type absorption modes in plate heat exchanger absorber design. Goel and Goswami [9] analytically investigated the combined heat and mass transfer process in a counter-current ammonia-water based lamella plate type absorber using empirical heat and mass transfer coefficients correlations.

In this study, a one-dimensional analytical model for microchannel absorber for absorption based electronics cooling system is developed. It is tailored to the analysis of the electronics cooling system which keeps the chip junction temperature near room temperature, while removing 100 W of heat load. An air-cooled microchannel absorber incorporated with off-set-strip-fin array for air-side heat transfer enhancement is investigated as a simpler alternative to liquid-cooled microchannel absorber. The working fluid is the water/LiBr pair, where water and LiBr are used as refrigerant and absorbent, respectively. To estimate the absorber performance at reference operating condition, the variations of LiBr mass fractions, mass flow rates and temperatures are inside microchannel absorber are investigated. Parametric study is also carried out to study the effects of the inlet temperature and mass flow rate of the coolant and inlet temperature of LiBr solution.

2. Principal features of system and absorber configurations

Fig. 1 shows a schematic diagram of an absorption-based heat pump system. Its main components include an evaporator, an absorber, a desorber, a condenser, a liquid pump and expansion devices. One of the major advantages of an absorption-based heat pump system is the utilization of low quality waste heat at a source temperature of around 90°C, which brings about significant reduction in operating costs and energy savings. The only component of this system with moving mechanical parts is the liquid pump, so that quiet operation is possible and no lubricant is needed. The coefficient of performance (COP) of an absorption-based heat pump system is defined as the heat removal capability of evaporator (q_e) per heat/power supply to desorber (q_d), i.e.,

$$\mathrm{COP} = \frac{q_e}{q_d} \tag{1}$$

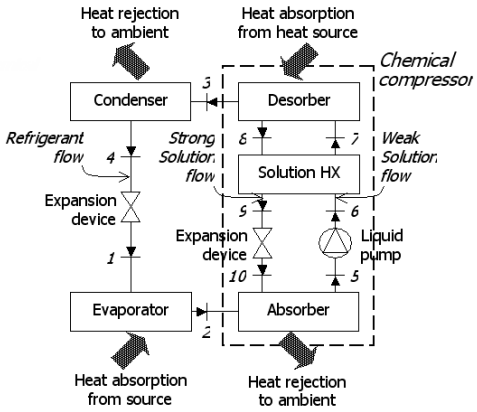

Fig. 1. Schematic diagram of an absorption-based heat pump system.

Power consumption of a liquid pump is usually negligibly small and neglected in Eq. (1) [10].

As shown in Fig. 1, the vapor compression refrigeration/heat pump system is similar to the absorption refrigeration/heat pump system, except the vapor compressor is replaced with a chemical compressor. The pressurization process in the chemical compressor starts in the absorber, where the refrigerant vapor from the evaporator (state point 2, Fig. 1) is exothermically condensed and absorbed into the strong LiBr solution (state point 10), resulting in a weak LiBr solution at the state point 5. Following the absorber, the LiBr solution is pressurized by the liquid pump to reach state 6. The solution heat exchanger preheats the weak LiBr solution of state point 6 to state point 7 using high temperature strong LiBr solution flowing from the desorber. In the desorber, high pressure and high temperature superheated refrigerant water vapor is generated (desorbed) from the weak LiBr solution and is returned to the refrigerant loop. At this point, the LiBr solution becomes strong again and returns to the absorber through the solution heat exchanger and an expansion device in sequence. This completes the solution loop of the chemical compression cycle.

Condensation in the condenser is associated with heat transfer and absorption associated with mass transfer in an absorber are the essential processes to make use of liquid pumps for pressurization, and thus to realize the chemical compression, as well as the miniaturization of the absorption based electronics cooling system. Fig. 2 shows the conceptual diagrams of the liquid-cooled and air-cooled absorbers. It is shown that the refrigerant (water) vapor flows through the inner channels and the aqueous LiBr solution counter-currently flows along the outer channel wall. Most of the heat generated during the absorption process is rejected to the coolant through the cold plate in a liquid-cooled absorber or via the offset-strip-fin array in an air-cooled absorber. A liquid cooling scheme using a cold plate provides higher heat transfer coefficient and lower coolant temperature than air cooling, leading to improved absorber performance. However, since the heat transferred to the liquid coolant must be rejected into ambient, an additional liquid-to-air heat exchanger needs to be used in the system which is not favorable to miniaturization.

An offset-strip-fin array with staggered structure of short strips can be used to enable an air-cooled absorber. A laminar boundary layer of air flow is developed on the short strip length, followed by its dispersion in the wake region between the strips [11]. Thus, the higher heat transfer coefficients of the laminar developing wake region can be exploited to enhance the air-side heat transfer. At $\mathrm{Re}_{d_h} = 1{,}000$, the Colburn j factor ($j = \mathrm{St}\,\mathrm{Pr}^{2/3}$) of the offset-strip-fin is 2.5 times higher than that of the plain fin, at the expense of the friction factor increase threefold [11]. Consequently, a significantly large heat transfer area with the enhanced heat transfer coefficients provided by the offset-strip-fin array makes the overall heat transfer (UA) of air cooling heat transfer comparable to that of liquid cooling heat transfer. The space and cost benefits from an air-cooled absorber can be possibly attractive relative to use of a liquid-cooled absorber, and therefore, a quantitative comparison between the liquid-cooled and air-cooled absorber is

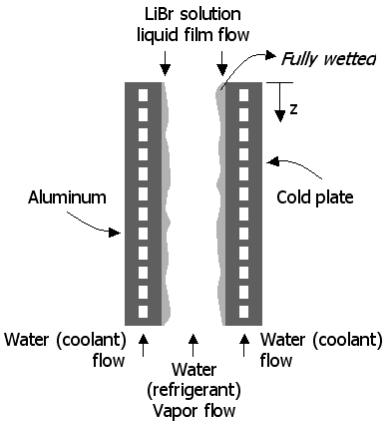

(a) Liquid-cooled microchannel absorber

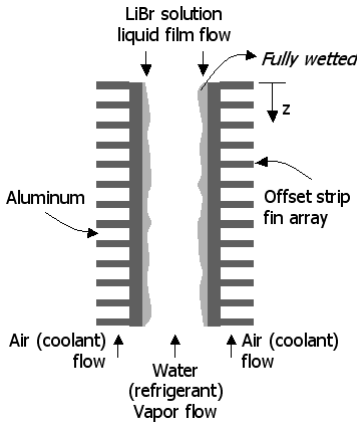

(b) Air-cooled microchannel absorber

Fig. 2. Conceptual diagrams of (a) liquid-cooled and (b) air-cooled microchannel absorber.

Table 1. Dimensions of microchannel absorbers.

Liquid-cooled absorber		Air-cooled absorber	
Solution channel		Solution channel	
Width, mm	10	Width, mm	10
Depth, mm	0.3	Depth, mm	0.3
Length, mm	100	Length, mm	100
Wall thickness, mm	0.3	Wall thickness, mm	0.3
Number of channels	10	Number of channels	10
Offset-strip-fin		Coolant channel	
Width, mm	0.5	Width, mm	2.1
Height, mm	0.3	Height, mm	22
Strip length, mm	32.5	Strip length, mm	32.5
Thickness, mm	0.3	Thickness, mm	0.7
Number of fins	129	Number of channels	37
Absorber length, mm	100	Absorber length, mm	100
Absorber width, mm	103.5	Absorber width, mm	103.5
Material	Aluminum	Material	Aluminum

carried out in this work. The dimensions of liquid-cooled and air-cooled absorbers investigated are listed in Table 1.

3. Model description

Considering the process diagrams in Figs. 2 and 3 and the dimensions listed in Table 1, we modified the predictive model of Goel and Goswami [9] for the liquid-cooled and air-cooled water-LiBr microchannel absorber. It is assumed that the cooling plate is fully wet by the liquid film so that no direct contact or heat exchange between the refrigerant vapor and cooling plate is allowed and thermodynamic equilibrium exists at the interface between aqueous LiBr solution and refrigerant (water) vapor. Also, mass transfer driven by thermal and pressure difference is regarded to be negligible. The effects of heat losses and non-condensable gases are not considered.

For steady state, the local refrigerant vapor absorption rate can be expressed in terms of an overall mass transfer coefficient, κ_s, and the concentration difference

$$-\frac{d\dot{m}_r}{dz}=\frac{d\dot{m}_s}{dz}=\tilde{P}_s\kappa_s\rho_s\left(x_s-x_i\right) \tag{2}$$

Several correlations for liquid film mass transfer coefficient are reviewed by Yih [12], and the correlation of Carrubba [12] is adopted here. For

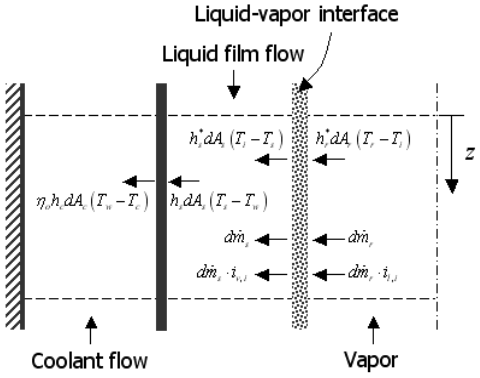

Fig. 3. Control volume for numerical simulations of microchannel absorber.

$40 < \mathrm{Re}_{\mathrm{film}} < 280$ and $\mathrm{Sc} \le 2.13\times10^5/\mathrm{Re}_{\mathrm{film}}^{1.6}$, the mass transfer coefficient is given by

$$\kappa_s = 3.7522\,\mathrm{Re}_{film}^{-\frac{1}{3}}\frac{D_{AB}}{\delta_r} \tag{3}$$

where the reduced film thickness, δ_r, is calculated from

$$\delta_r=\left(\frac{\nu^2}{g}\right)^{1/3} \tag{4}$$

The concentration conservation can be expressed by the statement that the mass of LiBr dissolved in solution is invariant, i.e.,

$$\frac{d}{dz}\left(\dot{m}_s x_s\right)=0 \tag{5}$$

On the refrigerant vapor side, sensible heat transfer from the liquid-vapor interface is balanced by the energy transport due to the refrigerant vapor absorption at the interface, which is responsible for the energy state of the remained vapor. Meanwhile, at liquid solution film, some vapor is condensed and absorbed into flowing solution with some of the heat transferred at the liquid-vapor interface and some rejected to the cooling plate. At the liquid-vapor interface, due to the exothermic absorption process, heat is transferred to both liquid and vapor driven by the local temperature difference, and also the loss of its energy occurs with the mass leaving the interface of the liquid solution film. The lost energy, however, is balanced by the mass/energy influx from refrigerant vapor. Eqs. (6)-(8) represent the energy conservation equations for refrigerant vapor, liquid film solution

and liquid-vapor interface, respectively.

$$\frac{d\left(\dot{m}_r i_r\right)}{dz} = h_r^* \tilde{P}_r \left(T_i - T_r\right) + \frac{d\dot{m}_r}{dz} i_{i,v} \tag{6}$$

$$\frac{d\left(\dot{m}_s i_s\right)}{dz} = h_s \tilde{P}_s \left(T_w - T_s\right) + h_s^* \tilde{P}_s \left(T_i - T_s\right) + \frac{d\dot{m}_s}{dz} i_{i,l} \tag{7}$$

$$\frac{d\dot{m}_s}{dz} i_{i,l} + \frac{d\dot{m}_r}{dz} i_{i,v} = h_s^* \tilde{P}_s \left(T_s - T_i\right) + h_r^* \tilde{P}_r \left(T_r - T_i\right) \tag{8}$$

The convective heat transfer coefficient between refrigerant vapor and the liquid-vapor interface can be determined from the Nusselt number correlation for laminar flow between parallel plates [13].

$$h_r = 8.235\left(\frac{k_r}{d_{h,r}}\right) \tag{9}$$

Heat transfer coefficient between the cooling plate and liquid film is determined by the correlation of Wilke [14].

$$h_s = 1.88\left(\frac{k_s}{\delta}\right) \quad \text{for} \quad \mathrm{Re}_{\mathrm{film}} < 2460\,\mathrm{Pr}^{-0.646} \tag{10}$$

where δ is the mean film thickness, which is calculated as follows, for laminar flow

$$\delta = \left(\frac{3\mu\Gamma}{\rho^2 g}\right)^{\frac{1}{3}} \tag{11}$$

The heat transfer coefficient between liquid film and liquid-vapor interface can be obtained by using heat and mass transfer analogy, [13]

$$h = \kappa\rho c_p \mathrm{Le}^{\frac{2}{3}} = \kappa\rho c_p \left(\frac{\mathrm{Sc}}{\mathrm{Pr}}\right)^{\frac{2}{3}} \tag{12}$$

As a first approximation to account for mass transfer at the interface, the heat transfer coefficients given by Eqs. (9) and (12) should be modified [15],

$$h^* = \frac{Nc_p}{1 - e^{-\frac{Nc_p}{h}}} \tag{13}$$

The energy conservation equation for coolant flow is given by

$$\dot{m}_c \frac{di_c}{dz} - \eta_o h_c \tilde{P}_c \left(T_w - T_c\right) = 0 \tag{14a}$$

$$\eta_o = 1 - \frac{A_f}{A_t}\left(1 - \eta_f\right) \tag{14b}$$

where η_f and η_o is the fin efficiency and overall surface efficiency, respectively.

For liquid-cooled absorber, the heat transfer coefficient of the coolant is evaluated by using the laminar flow convective heat transfer coefficient correlation from Shah and London [16] for the rectangular channel,

$$\mathrm{Nu} = 8.235\left(1 - 2.042\beta + 3.085\beta^2 - 2.477\beta^3 + 1.058\beta^4 - 0.186\beta^5\right) \tag{15}$$

Manglik and Bergles [17] proposed correlations to predict the j and f factors using Reynolds numbers and geometric parameters of the offset-strip-fins, which can be used to determine heat transfer coefficients and pressure drop in the air-cooled absorber. The laminar region correlations are given by

$$j = 0.652\,\mathrm{Re}_{d_{h,c}}^{-0.540}\left(\frac{s}{b}\right)^{-0.154}\left(\frac{t}{L_p}\right)^{0.150}\left(\frac{t}{s}\right)^{-0.068} \tag{16}$$

$$f = 9.624\,\mathrm{Re}_{d_{h,c}}^{-0.742}\left(\frac{s}{b}\right)^{-0.186}\left(\frac{t}{L_p}\right)^{0.305}\left(\frac{t}{s}\right)^{-0.266} \tag{17}$$

where the hydraulic diameter of the offset-strip-fin is defined by

$$d_{h,c} = \frac{4sbL_p}{\left[2\left(sL_p + bL_p + tb\right) + ts\right]} \tag{18}$$

The friction factor from Eq. (17) should be incorporated into Eq. (19), to evaluate the air-side pressure drop for the air flow in the offset-strip-fin array.

$$-\left(\frac{dP}{dz}\right) = \frac{2 f_c G_c^2}{d_{h,c}\rho_c} \tag{19}$$

The governing differential Equations (12)-(19) are first integrated and then discretized by using an upwind scheme [18]. Since, at the end of absorption process, the mass flow rate and thus Peclet number (Pe) of refrigerant vapor is small enough, making diffusion significant, a hybrid scheme is used for descritization of the vapor energy balance Eq. (6) [18]. The discretized equations are simultaneously solved iteratively, using a successive-under-relaxation (SUR) algorithm. The properties for LiBr solution are evaluated with data from Yuan and Herold [19], and the properties of water are determined by using

REFPROP 6.0 [20].

The heat transfer rates of LiBr solution side and refrigerant side inside microchannel absorbers can be evaluated by the following equations.

$$q_c = \int_0^L \eta_o h_c \tilde{P}_c \left(T_w - T_c\right) dz \tag{20}$$

$$q_{sen,l} = \int_0^L h_s^* \tilde{P}_s \left(T_i - T_s\right) dz \tag{21}$$

$$q_{latent,l} = \int_0^L i_{i,l} \tilde{P}_s \kappa_s \rho_s \left(x_s - x_i\right) dz \tag{22}$$

$$q_{sen,v} = \int_0^L h_r^* \tilde{P}_r \left(T_r - T_i\right) dz \tag{23}$$

$$q_{latent,v} = \int_0^L i_{i,v} \tilde{P}_s \kappa_s \rho_s \left(x_s - x_i\right) dz \tag{24}$$

The average thermal resistances of liquid phase (LiBr solution side) and vapor phase (refrigerant side) can be obtained by dividing average temperature differences between the phases and the interface by the sums of sensible and latent heat transfer rates of each phase, respectively.

$$R_{ave} = \frac{\frac{1}{L}\int_0^L \left(T_i - T_{r\ or\ s}\right) dz}{\left(q_{sen} + q_{latent}\right)} \tag{25}$$

4. Results and discussion

4.1 Performance of liquid-cooled and air-cooled microchannel absorbers under reference operating condition

The operating conditions used in simulations are given in Table 2. Figs. 4 and 5 show the overall performance of air-cooled and liquid-cooled microchannel absorbers, respectively, under the reference operating conditions at which it is designated that the absorption process is completed and the refrigerant mass flow rate vanishes at the inlet of LiBr solution flow (at z = 0 mm). The LiBr solution, which is introduced to the microchannel absorber as a saturated liquid, loses its energy to the coolant, leading to its temperature drop to become a subcooled liquid, whereas the liquid-vapor equilibrium at the phase interface is sustained by the continuous vapor influx. In consequence, the concentration of LiBr solution deviates from that of phase interface due to the temperature difference between the subcooled liquid and the saturated phase interface, which is plotted in Figs. 4a and 5a. The mass transfer and thus mass flow rate changes in Figs. 4b and 5b are induced by the concentration difference between the subcooled liquid and the saturated phase interface. The liquid solution ab-

Table 2. Operating conditions of microchannel absorbers.

Parameters	Values
Solution inlet flow rate, g/s	0.254
Solution inlet temp., °C	40/41/42.5*/44/45
Solution pressure, Pa	2914
Solution inlet LiBr mass fraction	Saturated liquid at T_{so} and P_s
Refrigerant inlet flow rate, g/s	0.042
Refrigerant inlet temp., °C	23.6
Refrigerant pressure, Pa	2914
Coolant flow rate, g/s (liquid-cooled)	2.5*
Air inlet velocity, m/s (air-cooled)	4.0/5.0/6.0*/7.0/8.0
Coolant inlet temp., °C	28/29/30*/31/32

* Reference operating conditions.

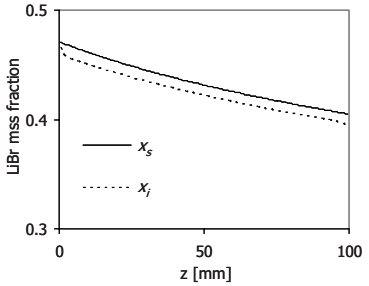

(a) LiBr mass fraction

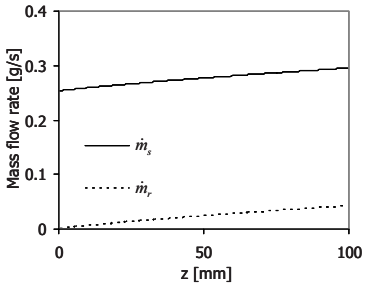

(b) Mass flow rate

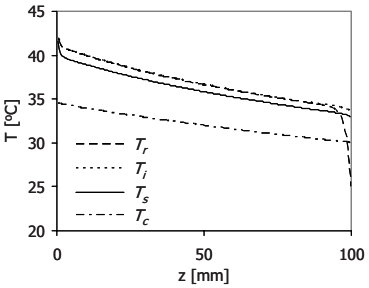

(c) Temperature

Fig. 4. (a) LiBr mass fraction, (b) mass flow rate and (c) temperature variations of air-cooled microchannel absorber under reference operating condition.

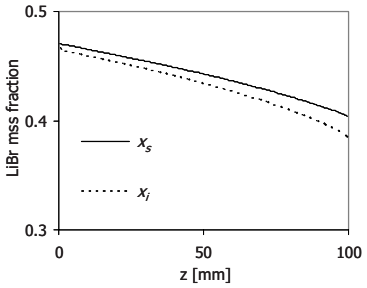

(a) LiBr mass fraction

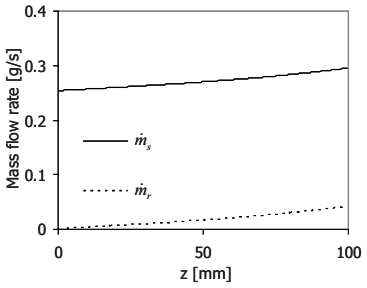

(b) Mass flow rate

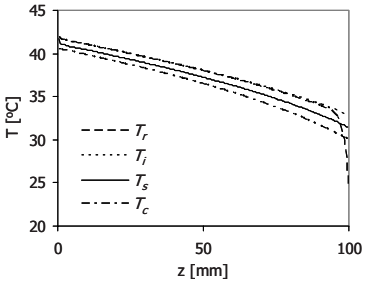

(c) Temperature

Fig. 5. (a) LiBr mass fraction, (b) mass flow rate and (c) temperature variations of liquid-cooled microchannel absorber under reference operating condition.

sorbs the refrigerant vapor and gradually increases, while the refrigerant vapor is condensed and eventually phased out at the inlet of the LiBr solution flow.

The latent heat released during the condensation/absorption process at the phase interface is mostly rejected to the coolant through liquid film and in turn cold plate of the liquid-cooled absorber or offset-strip-fin of air-cooled absorber. The temperature of the coolant that flows counter-currently to the solution flow, therefore, increases, while the temperature of the solution decreases along the absorber length. The refrigerant vapor gains some of the generated heat as well. Thus, the temperature of the refrigerant vapor rapidly approaches the interface temperature in Figs. 4(c) and 5(c). This implies that the amount of heat transferred to the refrigerant vapor is not very significant and the vapor side heat transfer resistance is negligible.

Overall comparison of results depicted in Figs. 4 and 5 shows that the performance of air cooling (U_c = 6 m/s, $\mathrm{Re}_{dh,c}$ = 1406) with the aid of offset-strip-fin array is comparable to that of liquid cooling ($\dot{m}_s$ = 2.5 g/s). It is observed that the mean temperature difference between the coolant and the LiBr solution in an air-cooled absorber is greater than that in the liquid-cooled absorber, which implies that liquid-cooled absorber still has more cooling potential than air-cooled absorber. However, it should be noted that the liquid-cooled absorber needs an additional liquid-to-air heat exchanger, making the air-cooled absorber more favorable to miniaturization. The overall heat rejections from the liquid-cooled and the air-cooled absorbers to the coolants are 110.7 W and 108.6 W, respectively. The air-side pressure drop through the offset-strip-fin array is calculated to be 64.6 Pa, which is negligibly small.

4.2 Performance of air-cooled microchannel absorber under various operating conditions

The air-side heat removal capability of the absorber can be enhanced by increasing the coolant (air) flow rate and/or temperature difference between LiBr solution and coolant (air). Therefore, the air inlet velocity, the air inlet temperature and the LiBr solution inlet temperature are the adjusting parameters which can control the air-side cooling capability. Higher air inlet velocity, lower air inlet temperature and/or higher LiBr inlet solution temperature provide greater cooling potential. The increased cooling capability contributes to reducing the overall temperature of the LiBr solution to coolant temperature so that the LiBr solution temperature is kept to be apart from its saturation temperature and liquid-vapor interface temperature. It is verified from Fig. 6, which illustrates the effects of those adjusting parameters on the temperatures of air-cooled micro-channel absorber. When the air inlet velocity increases from 4 m/s to 6 m/s, the average temperature of LiBr solution is reduced from 36.9°C to 36.1°C, leading to augmentation of average temperature difference between LiBr solution and liquid-vapor interface. Similar trends are observed from Figs. 6(b) and 6(c. Reducing air inlet temperature from 32°C to 30°C, the LiBr solution average temperature reduces by 0.95°C and thus the average

temperature difference between LiBr solution and interface is increased by 0.14°C. The increase of solution temperature from 40°C to 41.5°C also augments the cooling potential by adding 0.95°C of temperature difference between the LiBr solution and liquid-vapor interface.

Unique temperature behaviors are observed from Fig. 6 when the adjusting parameters are set to provide excessive cooling potential at which the effective absorption length is less than the absorber length. The LiBr solution temperature rapidly decreases and reaches its pinch point; it then remains constant along with the coolant temperature until the LiBr solution meets the counter-currently flowing refrigerant vapor, and thereby the condensation/absorption process takes place. Since there is no contribution of the latent heat generated during the condensation/absorption process to the heat transfer, LiBr solution loses its own energy more easily to coolant. Moreover, the heat transfer coefficient of LiBr solution flow in microchannel absorber is more than 10,000 W/m^{2}K and the solution mass flow rate is only 1% of coolant (air) mass flow rate at air velocity of 8 m/s so that the heat transfer between LiBr solution and coolant is significantly accelerated. Once the absorption process occurs, the interface temperature is drastically separated from the LiBr solution temperature in very high degree of subcooling to its liquid-vapor equilibrium temperature with the release of latent heat.

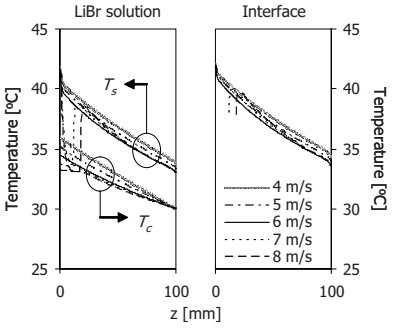

(a) Air inlet velocity

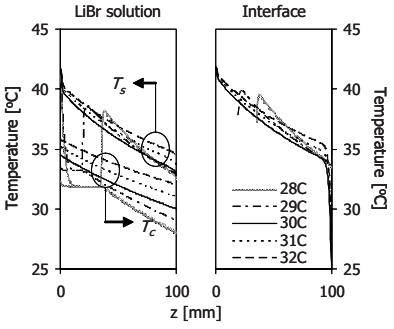

(b) Air inlet temperature

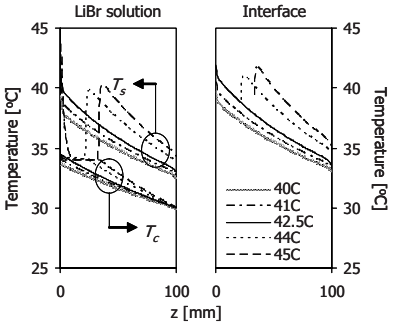

(c) Solution inlet temperature

Fig. 6. Effects of (a) air inlet velocity, (b) air inlet temperature, and (c) LiBr solution inlet temperature on temperature of the LiBr liquid solution, liquid-vapor interface and coolant (air) in the air-cooled microchannel absorber for the dimensions and operating conditions listed in Table 2.

The temperature variations induced by the air-side cooling capability variations directly affect the LiBr concentration of the LiBr solution and liquid-vapor interface, which is the driving force of the mass transfer from refrigerant vapor to LiBr solution. Fig. 7 shows how the air inlet velocity, air inlet temperature and LiBr solution inlet temperature affect the mass flow rate of the LiBr solution and refrigerant vapor. As expected, the augmentation of air-side cooling capability accelerates the absorption rate and thus reduces the effective absorption length. When the air inlet velocity of 8 m/s was supplied, the effective absorption length was only 82.3 mm, while for the air inlet velocity of 4 m/s, the refrigerant mass flow rate of 0.006 g/s (13.5% of introduced refrigerant vapor flow rate) escaped from the absorber as an unabsorbed vapor. Also, Fig. 7b shows that the increase of air inlet temperature by 4°C leads to the decrease of average absorption rate per unit length, which is defined as the total absorbed refrigerant vapor mass flow rate divided by the microchannel absorber length (L = 10 cm), from 0.61 g/m·s to 0.34 g/m·s as listed in Table 3. The effective absorption length for the LiBr solution inlet temperature of 28°C is only 45.75 mm, while for the LiBr solution inlet temperature of 32°C, 116.99 mm of absorption length is expected to be necessary for the complete absorption. The LiBr solution inlet temperature has a significant effect on the mass transfer as well. When the LiBr solution inlet temperature changes from 40°C to 45°C, the average

Table 3. Refrigerant average absorption rates per unit length inside air-cooled microchannel absorber.

U_c, m/s	γ_{ave}, g/m·s	T_c, °C	γ_{ave}, g/m·s	T_s, °C	γ_{ave}, g/m·s
4	0.36	28	0.61	40	0.34
5	0.39	29	0.51	41	0.37
6	0.41	30	0.41	42.5	0.41
7	0.46	31	0.38	44	0.53
8	0.50	32	0.34	45	0.60

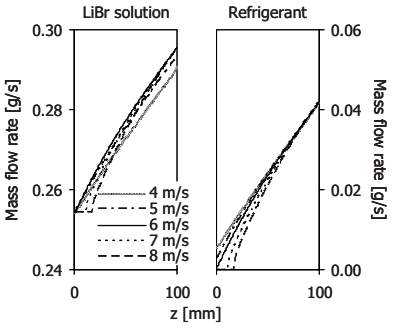

(a) Air inlet velocity

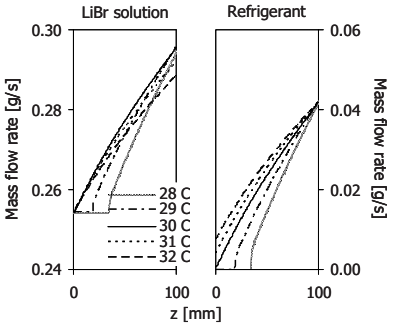

(b) Air inlet temperature

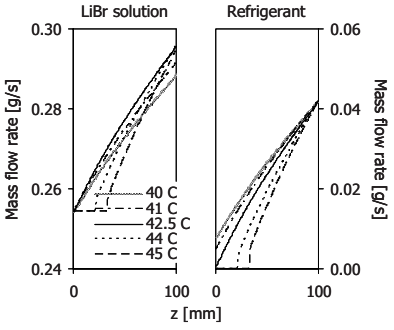

(c) Solution inlet temperature

Fig. 7. Effects of (a) air inlet velocity, (b) air inlet temperature, and (c) LiBr solution inlet temperature on mass flow rates of the LiBr liquid solution and refrigerant in the air-cooled microchannel absorber for the dimensions and operating conditions listed in Table 2.

absorption rate per unit length increases from 0.34 g/m·s to 0.60 g/m·s. It is possible to deduce that the air inlet temperature has a stronger influence on the absorption rate than the LiBr solution inlet temperature. In summary, the enhanced heat transfer capability keeps the LiBr solution temperature well below its saturation temperature and liquid-vapor interface temperature so that the absorber performance can be enhanced, along with the transfer and absorption rates.

Fig. 8 shows the heat transfer network inside microchannel absorber, and Table 4 lists the corresponding heat transfer rates and average thermal resistances. Thermal resistance is evaluated considering both sensible heat transfer driven by temperature difference and latent heat transfer driven by mass transfer. The thermal resistance of liquid phase is around three-times larger than that of the vapor phase, making the heat transfer resistance of the vapor phase negligible. Also, it can be found that in refrigerant vapor most of the heat transfer is carried out by the latent heat transfer from refrigerant vapor to the phase interface, while sensible heat transfer is the major mechanism in LiBr solution. Absorber cooling capacities are also listed in Table 4. Due to the unabsorbed refrigerant vapor, under the operating conditions of low cooling potential, which corresponds to low air inlet velocity, high air inlet temperature and low solution inlet temperature, the required cooling power, is smaller than that in the reference operating condition. For the operating conditions of high cooling potential, less cooling power is consumed than reference operating condition as well. More efficient absorption driven by high cooling potential can be one of the possible explanations for the reduced cooling power consumption. The pressure drop of air flow through the offset-strip-fin array is almost invariant to the air and solution inlet temperature variations, while it is proportional to the air inlet velocity increase. The maximum pressure drop calculated was 92.5 Pa.

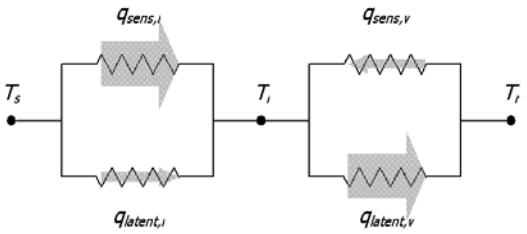

Fig. 8. Heat transfer network inside microchannel absorber.

Table 4. Heat transfer rates and average thermal resistances inside air-cooled microchannel absorber.

U_c	q_c	$q_{sen,l}$	$q_{latent,l}$	$R_{ave,l}$	$q_{sen,v}$	$q_{latent,v}$	$R_{ave,l}$
4	95.4	89.6	2.71	7.71	-1.14	93.5	2.37
5	102.9	96.8	2.88	7.70	-1.09	100.8	2.11
6	108.6	102.3	3.01	7.70	-1.05	106.4	1.93
7	105.9	99.7	2.96	7.66	-1.04	103.6	1.95
8	105.5	99.3	2.93	7.64	-1.03	103.2	1.95
T_c	q_c	$q_{sen,l}$	$q_{latent,l}$	$R_{ave,l}$	$q_{sen,v}$	$q_{latent,v}$	$R_{ave,l}$
28	101.2	94.7	2.81	7.59	-1.02	98.5	2.02
29	105.3	98.9	2.94	7.64	-1.03	102.8	1.95
30	108.6	102.3	3.01	7.70	-1.05	106.4	1.93
31	99.2	93.4	2.80	7.71	-1.11	97.3	2.23
32	90.0	84.6	2.58	7.71	-1.17	88.4	2.58
T_s	q_c	$q_{sen,l}$	$q_{latent,l}$	$R_{ave,l}$	$q_{sen,v}$	$q_{latent,v}$	$R_{ave,l}$
40	89.2	84.4	2.39	7.67	-1.00	87.8	2.23
41	97.1	91.7	2.64	7.68	-1.03	95.4	2.10
42.5	108.6	102.3	3.01	7.70	-1.05	106.4	1.93
44	105.1	98.2	3.05	7.66	-1.12	102.4	2.13
45	102.2	95.0	3.02	7.64	-1.18	99.2	2.31

5. Conclusion

The performance of air-cooled and liquid-cooled microchannel absorbers is numerically evaluated and discussed. The results showed that an air-cooled microchannel absorber incorporated with an offset-strip-fin array can have comparable performance to a liquid-cooled microchannel absorber. It can be concluded from parametric study that absorber performance is significantly affected by the cooling capability of coolant, which can be controlled by air inlet velocity, air inlet temperature and solution inlet temperature. It is found that LiBr solution predominantly controls both the heat transfer and mass transfer mechanisms in the absorption process. The major heat transfer mechanism in the vapor phase is identified to be latent heat transfer, while in liquid phase, sensible heat transfer is the dominant mechanism. The pressure drop of air flow through the offset-strip-fin array is only affected by the air inlet velocity. At reference operating condition, the pressure drop was calculated to be 64.6 Pa and the maximum pressure drop at air inlet velocity of 8 m/s was 92.5 Pa.

Acknowledgment

The authors gratefully acknowledge the support of the Korea Research Foundation Grant funded by the Korean Government (MOEHRD) (KRF- 2005-214-D00232) and Interconnect Focus Center, one of the research centers funded under the Focus Center Research Program, a Semiconductor Research Corporation Program.

Nomenclature

A_f : Finned surface area, [m^2]
A_t : Total exposed surface area [m^2]
b : Fin height, [m]
COP : Coefficient of performance
c_p : Specific heat, [J/kg·K]
D_{AB} : Diffusion coefficient from liquid A to Liquid B, [m/s]
d_h : Hydraulic diameter, [m]
f : Friction factor
g : Gravitational acceleration, [m/s^2]
G : Mass flux, [kg/m^2s]
h : Convective heat transfer coefficient, [$W/m^2 \cdot K$]
i : Specific enthalpy, [J/kg]
j : Colburn j factor, $\mathrm{St}\,\mathrm{Pr}^{2/3}$
k : Thermal conductivity, [W/m·K]
L : Microchannel absorber length, [m]
Le : Lewis number, $\frac{\alpha}{D_{AB}}$
L_p : Strip flow length of offset-strip-fin, [m]
$\dot{m}$: Mass flow rate, [kg/s]
N : Mass flux at the phase interface, [$kg/m^2 \cdot s$]
Nu : Nusselt number, $\frac{hd_h}{k}$
P : Pressure, [Pa]
$\tilde{P}$: Perimeter, [m]
Pe : Peclet number, $\frac{d_h u}{\alpha}$
Pr : Prandtl number, $\frac{\nu}{\alpha}$
q : Heat transfer rate, [W]
R : Thermal resistance, [K/kW]
Re : Reynolds number, $\frac{\rho u d_h}{\mu}$
$\mathrm{Re}_{\mathrm{film}}$: Reynolds number for falling film, $\frac{4\Gamma}{\mu}$
s : Channel or fin pitch, [m]
Sc : Schmidt number, $\frac{\nu}{D_{AB}}$
St : Stanton number, $\frac{h}{\rho u c_p}$

t : Fin thickness, [m]
T : Temperature, [K]
U : Overall heat transfer coefficient [W/m^{2}K] or velocity, [m/s]
x : Mass fraction of LiBr
z : Axial coordinate, [m]

Greeks

α : Thermal diffusivity, [m^2/s]
β : Aspect ratio, $\frac{s}{b}$
δ : Film or membrane thickness, [m]
Γ : Mass flow rate per wetted perimeter, [kg/m·s]
γ_{ave} : Average absorption rate per unit length, [g/m·s]
η_f : Fin efficiency
η_o : Overall surface efficiency
κ : Mass transfer coefficient, [m/s]
λ : Latent heat of vaporization, [J/kg]
μ : Dynamic viscosity, [Pa·s]
ν : Kinematic viscosity, [m^2/s]
ρ : Density, [kg/m^3]

Subscripts

a : Air
ave : Average
c : Coolant
d : Desorber
e : Evaporator
i : Interface
l : Liquid phase
latent : Latent heat
r : Refrigerant
s : Solution
sen : Sensible heat transfer
v : Vapor phase
w : Wall

Superscript

* : Modified

References

[1] International Technology Roadmap for Semiconductors, Assembly and Packaging, (2005) Ed.
[2] R. Mongia, K. Masahiro, E. DiStefano, J. Barry, W. Chen, M. Izenson, F. Possamai, A. Zimmermann and M. Mochizuki, Small scale refrigeration system for electronics cooling within a notebook computer, Proc. Tenth Intersociety Conference on Thermal and Thermomechanical Phenomena in Electronics Systems, San Diego, CA, USA. (2006) 751-758.
[3] M. K. Drost and M. Friedrich, Miniature heat pump for portable and distributed space conditioning applications, Proc. Thirty-Second Intersociety Energy Conversion Engineering Conference, Honolulu, Hawaii, USA, (1997) pt. 2, 1271-1274.
[4] A. Beutler, F. Ziegler and G. Alefeld, Falling film absorption with solutions of a hydroxide mixture, International Absorption Heat Pump Conference, Montreal, Canada, (1996) 303–309.
[5] J. D. Killion and S. Garimella, A critical review of models of coupled heat and mass transfer in falling film absorption, *Int. J. Refrigeration* 24 (2001) 755-797.
[6] V. Patnaik, H. Perez-Blanco and W. A. Ryan, A simple analytical model for the design of vertical tube absorbers, *ASHRAE Trans.* 99 (2) (1993) 81-89.
[7] J. M. Meacham and S. Garimella, Modeling of local measured heat and mass transfer variations in a microchannel ammonia-water absorber, *ASHRAE Trans.* 109 (2003) 412-422.
[8] Y. T. Kang, A. Akisawa and T. Kashiwagi, Analytical investigation of two different absorption modes: falling film and bubble types, *Int. J. Refrigeration* 23 (2000) 430-443.
[9] N. Goel and D. Y. Goswami, Analysis of a counterflow vapor flow absorber, *Int. J. Heat Mass Transfer* 48 (2005) 1283-1292.
[10] F. C. McQuiston, J. D. Parker and J. D. Spitler, Heating, Ventilating, and Air Conditioning: Analysis and Design, 5 ed., John Wiley & Sons, New York, (2000) 215.
[11] R. L. Webb, Principles of Enhanced Heat Transfer, John Wiley & Sons, New York, (1994) 89.
[12] S. M. Yih, Modeling heat and mass transfer in wavy and turbulent falling liquid films, *Wärme- und Stoffübertragung* 21 (1987) 373-381.
[13] F. P. Incropera and D. P. De Witt, Fundamentals of Heat and Mass Transfer, John Wiley & Sons, New York, (1990) 501.
[14] W. Wilke, Warmeubergang and rieselfilme, *VDI-Forschungsheft* 490 (1962) B28.
[15] R. E. Treybal, Mass Transfer Operation, McGraw-Hill, New York (1968) 67-70.

[16] R. K. Shah and A. L. London, Laminar flow forced convection in ducts, A Source Book for Compact Heat Exchanger Analytical Data, *Advances in Heat Transfer*. Academic Press, NewYork, (1978) Supplement 1.

[17] R. M. Manglik and A. E. Bergles, The thermal-hydraulic design of the rectangular offset-strip-fin compact heat exchangers, In: R. K. Shah, A. D. Kraus, and D. Metzger, editors. Compact Heat Exchangers. Hemisphere, Washington, (1994) 123-150.

[18] S. V. Patankar, Numerical Heat Transfer and Fluid Flow, Hemisphere, Washington DC, (1980).

[19] Z. Yuan and K. E. Herold, Thermodynamic Properties of Aqueous Lithium Bromide Using a Multiproperty Free Energy Correlation, *Int. J. Heating, Ventilating, Air-Conditioning and Refrigeration* 11 (3) (2005).

[20] M. O. McLinden, S. Klein, E. Lemmon and A. Peskin, NIST Thermodynamic and Transport Properties of Refrigerants and Refrigerant Mixtures Database (REFPROP), Version 6.0, National Institute of Standards and Technology, Gaithersburg, Maryland, USA, (1998).